Atmos. Chem. Phys. Discuss., doi:10.5194/acp-2015-922, 2016
Manuscript under review for journal Atmos. Chem. Phys.
Published: 15 January 2016

Atmospheric Chemistry and Physics Discussions

Simulated 2050 aviation radiative forcing

C.-C. Chen and A. Gettelman

National Center for Atmospheric Research, P.O. Box 3000, Boulder, CO 80307-3000, USA

Received: 12 November 2015 – Accepted: 17 November 2015 – Published: 15 January 2016

Correspondence to: C.-C. Chen (cchen@ucar.edu)

Published by Copernicus Publications on behalf of the European Geosciences Union.

Abstract

The radiative forcing from aviation is investigated by using a comprehensive general circulation model in the present (2006) and the future (through 2050). Global flight distance is projected to increase by a factor of 4 between 2006 and 2050. However, simulated contrail cirrus radiative forcing in 2050 can reach 87 mW m^{-2}, an increase by a factor of 7 from 2006, and thus does not scale linearly with fuel emission mass. This is due to non-uniform regional increase in air traffic and different sensitivities for contrail radiative forcing in different regions.

Simulations indicate that negative radiative forcing induced by the indirect effect of aviation sulfate aerosols on liquid clouds in 2050 can be as large as −160 mW m^{-2}, an increase by a factor of 4 from 2006. As a result, the net 2050 aviation radiative forcing has a cooling effect on the planet. Aviation sulfate aerosols emitted at cruise altitude can be transported down to the lower troposphere, increasing the aerosol concentration, thus increasing the cloud drop number concentration and persistence of low-level clouds. Aviation black carbon aerosols produce a negligible net forcing globally in 2006 and 2050.

1 Introduction

Aviation fossil fuel consumption is projected to increase significantly during the 21st century due to population and economic growth. Thus the aviation impact on climate is expected to intensify substantially from its current estimated level (IPCC, 1999; Lee et al., 2009) faster than other sources, and become a larger component of future radiative forcing than it is today. Since future population and economic growth are most likely non-uniform, some regions may experience higher aviation impact than others. For example, with the recent rapid development in Asia during the past decades, this region is likely to join central Europe and the eastern US with high regional aviation emissions.

ACPD
doi:10.5194/acp-2015-922

Aviation causes several important climate impacts. Linear contrails form when aircraft exhaust mixes with ambient air that is cold and moist enough (Schmidt, 1941; Appleman, 1953). Subsequently, spreading and shearing of contrails may increase cloudiness, called contrail cirrus (Schumann and Wendling, 1990; Minnis et al., 1998). Linear contrails and contrail cirrus produce a warming effect on the planet since the radiative forcing of these optically thin high clouds is dominated by longwave heating (Dietmüller et al., 2008; Rap et al., 2010). Nevertheless, it is a challenge to quantify the radiative forcing of contrail cirrus since this requires accurately accounting for the spreading of contrails. Based on some recent studies using general circulation model simulations, Burkhardt and Kärcher (2011) estimated present day contrail cirrus radiative forcing of 31 $mW\,m^{-2}$, Chen and Gettelman (2013) estimated 13 $mW\,m^{-2}$, and Schumann and Graf (2013) estimated 50 $mW\,m^{-2}$.

Aircraft also emit various aerosols, such as sulfate and Black Carbon (BC, or soot). In addition to directly absorbing and reflecting radiation, sulfate and BC can alter cloud properties, such as drop and crystal concentration, and cloudiness in the troposphere. These "indirect effects" of aviation aerosols may result in a change in cloud radiative forcing. Hendricks et al. (2005, 2011) found that aviation BC could significantly increase the crystal concentration if aviation BC could serve efficiently as ice nuclei. Furthermore, Penner et al. (2009) reported that aviation BC could induce an indirect forcing of $-161\,mW\,m^{-2}$ by assuming aviation BC as highly efficient heterogeneous ice nuclei. However, using a more typical ice nucleating efficiency of BC (DeMott et al., 2009, 2010, 0.1 %) and size distribution for aviation BC, Gettelman and Chen (2013) found negligible direct and indirect BC radiative forcing. Aviation sulfate aerosols, however, have been estimated to be producing at present a radiative forcing of $-46\,mW\,m^{-2}$, by altering the properties of warm clouds (Gettelman and Chen, 2013), e.g. drop concentration and liquid water path. Similar effects of aviation sulfate aerosols were reported by Righi et al. (2013). These values are larger than the potential warming effect of contrails and contrail cirrus.

ACPD
doi:10.5194/acp-2015-922

In this study, we will explore the future aviation impact on climate by employing a comprehensive general circulation model and four different future scenarios. We will focus on the radiative forcing induced by contrail cirrus and aviation aerosols: by far the most uncertain aviation radiative forcing components (Lee et al., 2009). Model description and future aviation emission scenarios are described in Sect. 2, model simulation results are presented in Sect. 3, and discussions are in Sect. 4.

2 Methodology

2.1 Model description

Community Atmosphere Model version 5 (CAM5) is employed in this study and a detailed scientific description can be found in Neale et al. (2010). The model includes a detailed treatment of liquid and ice cloud microphysics (Morrison and Gettelman, 2008), including a representation of particle size distributions, a detailed representation of mixed phase clouds with the consideration of water uptake onto ice (the Bergeron–Findeisen process) and ice supersaturation (Gettelman et al., 2010). This is coupled to a consistent radiative treatment of ice clouds, and an aerosol model (7-mode aerosol model employed in this study) that includes particle effects on liquid and ice clouds (Liu et al., 2012). This method has the advantage of being self-consistent with the climate simulation.

The evolution of BC and sulfate aerosols in CAM5 is described in detail in Liu et al. (2012). Briefly, BC is emitted to the primary carbon mode, then is aged into the accumulation mode by condensation of H_2SO_4, NH_3 and semi-volatile organics and by coagulation with Aitken and accumulation modes. BC and sulfate aerosols are internally mixed in the modes and the optical properties reflect this. Aviation aerosols are treated in the same manner, and simply added to the existing modal description. Activation of aerosols to ice nuclei is calculated by the activation scheme following Liu et al. (2009); Gettelman et al. (2010), with homogenous freezing on sulfate. It is assumed

ACPD
doi:10.5194/acp-2015-922

that 0.1 % of black carbon can be activated as heterogenous ice nuclei (Gettelman and Chen, 2013).

As shown in Chen et al. (2012), CAM5 is capable of simulating the mean relative humidity and reproducing the distribution of the frequency of ice supersaturation in the upper troposphere and lower stratosphere (UTLS) as observed from the Atmospheric Infra Red Sounder (AIRS) satellite (Gettelman et al., 2006). These attributes are critical in simulating contrails.

The contrail parameterization used in this study is described in detail in Chen et al. (2012). The parameterization follows the Schmidt–Appleman Criteria (Schmidt, 1941; Appleman, 1953) to determine if aviation water emissions should be vapor or condensed water (ice) depending on the ambient conditions. The implemention follows Ponater et al. (2002): contrails are initialized if aviation water vapor encounters an ambient condition with the atmospheric temperature below a critical temperature, as a function of atmospheric pressure, and the ambient humidity above ice supersaturation. Otherwise, the aviation water emission is added to the background water vapor.

We use the approximation of the critical temperature (T_c in °C) for contrail formation given by Schumann (1996)

$$T_c = -46.46 + 9.43\ln(G - 0.053) + 0.72[\ln(G - 0.053)]^2,$$

and G in the units of $\mathrm{Pa\,K^{-1}}$ is defined as

$$G = \frac{\mathrm{EI}_{H_2O} \cdot c_p \cdot p}{\varepsilon Q(1-\eta)},$$

where EI_{H_2O} is the emission index of water vapor, c_p the specific heat of air at constant pressure, p the atmospheric pressure, ε ratio of the molecular weight of water and air, Q the specific combustion heat, η the propulsion efficiency of the jet engine. In this study, $\mathrm{EI}_{H_2O} = 1.21$ ($\mathrm{kg\,H_2O\,kg^{-1}}$ fuel), $Q = 4.3 \times 10^7\ \mathrm{J\,kg^{-1}}$, $\eta = 0.3$.

One important assumption made in this parameterization is that the initial volume of contrails is a product of the flight path distance and a cross-sectional area, assumed to

ACPD
doi:10.5194/acp-2015-922

be 300 m × 300 m (Chen et al., 2012). The ambient humidity above ice saturation within this volume is assumed to become part of the contrail ice mass. Ice particles within contrails when initialized are assumed to be spherical and have an initial diameter of 10 µm (Schröder et al., 2000). Chen et al. (2012) discuss the sensitivity of contrail forcing to the choice of particle size and cross-sectional area. When a contrail is initialized, its cloud fraction is calculated by its volume and that of the grid box and we assume there is no overlap with the exisiting clouds within the grid box. After contrails are initialized, they become indistinguishable from the background cloud field, i.e. there is no separate cloud type for contrails in CAM5, and they evolve in the same manner as all clouds in CAM5.

2.2 Future aviation emissions scenarios

Four future aviation emission scenarios of identical flight tracks and flight distance are considered in this study, along with a present day scenario. Scenarios were developed by (Barrett et al., 2010) and are listed in Table 1.

Based on projected population and economic growth by 2050 with the current aviation technology, a "baseline" aviation emission scenario is obtained (BL). Scenario 1 (SC1) assumes the same 2050 flight distance with an assumption of 2 % gain in engine efficiency per year, which reduces fuel consumption with the same flight distance as BL. Scenario 2 (SC2) is obtained with SC1 fuel consumption by assuming an alternative fuel with no sulfate emissions and 50 % reduction in aviation BC emissions. Scenario 3 (SC3) is the same as Scenario 2 except an increase of 5 % in water vapor emission is assumed. Future aviation emissions based on these four scenarios are available for the years of 2016, 2026, 2036, and 2050. It is important to emphasize that the flight distance for any given year remains the same under all four scenarios, and just the fuel use varies.

As illustrated in Fig. 1, the global flight distance is projected to increase by a factor of 4 from 2006 to 2050 and the fuel consumption is projected to increase by a factor of 5 under BL and 2.7 under SC1 by 2050. The biggest increase in flight distance (a factor

ACPD
doi:10.5194/acp-2015-922

of 6 by 2050) is found in East Asia, due to the projected rapid economic growth in this region. The fractional increase in flight distance in central Europe is nearly the same as that of the global flight distance, while the increase in eastern US (a factor of 2.5 in 2050) is much lower.

2.3 Modeling framework and background meteorology

Following the methodology described in Gettelman and Chen (2013); Chen and Gettelman (2013), CAM5 with specified dynamics (CAM5-SD) is employed for this study. Future background meteorology is obtained from fully coupled simulations using Community Earth System Model (CESM) under Representative Concentration Pathways (RCPs) with radiative forcing in 2100 of 4.5 and 8.5 $\mathrm{W\,m^{-2}}$ (van Vuuren et al., 2011), hereafter RCP4.5 and RCP8.5. Future emissions from non-aviation sources and greenhouse gas concentration are based on RCPs for the respective year of the aviation emissions for CAM5-SD simulations. To address the uncertainty due to background meteorology, we use four different annual cycles from a CESM coupled experiment with a given RCP to drive CAM5-SD and perform 20 year SD simulations (repeating an annual cycle each year). For example, for 2050 aviation emissions, we use the background meteorologies from years 2049, 2050, 2051, and 2052 to drive CAM5-SD to form an ensemble. The radiative forcing is then estimated from 80 simulated years. All simulations presented in this study are run on a $1.9^{\circ} \times 2.5^{\circ}$ latitude–longitude grid with 30 vertical layers.

Due to global warming, atmospheric temperature at the cruise altitude is warmer under both RCP4.5 and RCP8.5 than present day meteorology. Note also that there are slight shifts in flight altitude as newer planes fly at higher altitude which is about 20 hPa lower in atmospheric pressure in 2050 than in 2006. The upper tropospheric warming reduces the frequency for contrail formation (Fig. 2). A potential contrail can form when the temperature and humidity satisfy the Schmidt–Appleman contrail formation criteria. Furthermore, if the atmosphere is supersaturated with respect to ice, the contrail will persist. The critical threshold temperature is the dominant factor in the Schmidt–

ACPD
doi:10.5194/acp-2015-922

Appleman Criteria (Schmidt, 1941; Appleman, 1953). Figure 2b and c indicate that future atmospheric conditions in the tropics and subtropics is less favorable for contrail formation at the cruise altitude, mainly due to higher atmospheric temperatures. The reduction in the frequency of persistent contrails over East Asia (Fig. 2e and f) has important implications since there is substantial projected increase in air traffic in this region. The reductions are larger in RCP8.5 than in RCP4.5 due to stronger warming. In mid and high latitudes at cruise altitude, however, future atmospheric conditions become more favorable for contrail formation (Fig. 2b and c). Figure 2e and f indicate that the frequency of persistent contrails in 2050 is increased slightly over eastern US and central Europe.

3 Results

Three sets of simulations are conducted in this study. The first set is the control simulation in which no aviation emissions are included. The second set of simulations include aviation water vapor emission only and thus the difference from the control run can be interpreted as the effect of contrails and contrail cirrus ("Contrail Cirrus" or "H_2O"). The third set of simulations include aviation water vapor, sulfate, and BC emissions, and thus the difference from the control run is due to the combination of contrail cirrus and aviation aerosols ("BC + SO_4 + H_2O"). Hence, the impact of aviation aerosols may be deduced by taking the difference between the second and third sets of simulations.

3.1 Global average

The radiative forcing of contrail cirrus in 2050 simulated by CAM5 ranges between 75 and 95 mW m^{-2} based on various aviation emission scenarios and different background meteorology (Fig. 3a). Based on our simulations, the highest radiative forcing of contrail cirrus (red dashed line in Fig. 3a) is reached when BL emission (higher fuel consumption) is incorporated with present-day meteorology. In other words, the effect

ACPD
doi:10.5194/acp-2015-922

of global warming, i.e. background meteorology under both RCPs, is to reduce radiative forcing of contrail cirrus. Conversely, the lowest radiative forcing (green solid line in Fig. 3a) can be obtained when SC1 emission (lower fuel consumption) is incorporated with background meteorology under RCP8.5 (warmest ambient temperatures at cruise altitude).

Figure 3a and Table 3 indicate that when considering global contrail cirrus RF only (no aerosol effects), the spread across emissions scenarios in 2050 is 73–83 mW m^{-2} (13 %, based on 2050 RCP8.5 meteorology), while the spread due to future meteorology (RCP4.5 v. RCP8.5) in 2050 is only 80–87 mW m^{-2} (8 %, based on 2050BL), thus the spread in scenarios (and total fuel burn) is more important than the climate scenarios (the degree of projected warming). Warmer worlds (RCP8.5) result in less contrail cirrus RF.

Figure 3b illustrates the combined radiative forcing of contrail cirrus and aviation aerosols. Clearly, the net effect is positive when aviation sulfate emission is eliminated (SC2 and SC3, blue and magenta lines in Fig. 3b), and these scenarios are nearly identical to the SC1 and SC3 contrail only results in Fig. 3a. The corresponding deduced aerosol forcing (blue and magenta lines in Fig. 3c), i.e. aviation BC, is nearly zero. Hence, the negative forcing is produced by aviation sulfate aerosols. Figure 3b illustrates that the sum of the negative forcing induced by aviation sulfate aerosols, aviation BC and contrail cirrus heating is negative, consistent with the findings by Gettelman and Chen (2013). The effects are larger (more cooling) for the 2050 BL case (red) than for SC1 (green), mostly due to the larger RF from aerosols (Fig. 3c). 5 % additional aviation water vapor emission is not significant in enhancing contrail radtiative forcing (see Fig. 3), since the magenta SC3 lines with enhanced aviation water are not significantly different from SC2.

3.2 Zonal mean perturbations

Figure 4 presents zonally averaged perturbations due to 2050 aviation emissions with 2050 meteorology under RCP8.5, highlighting the difference between the effects of

ACPD
doi:10.5194/acp-2015-922

contrails through aviation emissions of water ("H_2O": green in Fig. 4) and the effects of water and aerosols ($H_2O + SO_4 + BC$: blue in Fig. 4). The effect of water is only significant when the water condenses as contrail or contrail cirrus: the direct RF of aviation water vapor is not significant, as seen in Fig. 3 and noted by Chen et al. (2012). Aviation aerosols are found to enhance both the negative shortwave cloud forcing (Fig. 4a) and positive longwave cloud forcing (Fig. 4b), with a larger effect on the shortwave. The net forcing of aviation becomes mostly negative (Fig. 4c). The aerosol effects on the cloud forcing arise mainly through enhancing cloud drop number concentration (Fig. 4e) and liquid water path (Fig. 4g), which are not significantly affected by aviation H_2O forming contrails. Cloud top ice number concentration increases by aviation are enhanced with aerosols (Fig. 4f) which in turn raises ice water path more than water emissions do alone. As expected, these effects are mainly found in the mid and high latitudes in the Northern Hemisphere where the most significant aviation emissions occur. As seen in the global averages (Fig. 3c), for SC2, with no sulfur, aviation BC produces a negligible radiative forcing, and thus most of the negative radiative forcing is due to aviation sulfate aerosols.

Perturbations produced by different aviation emissions scenarios are shown in Fig. 5. These simulations include aviation water vapor, sulfate and BC emissions. SC3 is not significantly different from SC2, so it is not shown. Baseline emissions (blue) are the same in Fig. 4 and Fig. 5. The largest magnitude shortwave and longwave cloud forcings, are produced by the 2050 BL (largest fuel consumption). However, the largest net cloud forcing (Fig. 5c), is produced by the 2050 Scenario 2 emissions, which has a lower amount of fuel consumption than the 2050 BL. But SC2 has no sulfate emissions, and so the cooling effect resulting from aviation sulfate aerosols (in the shortwave cloud radiative effect, Fig. 5a) is removed.

The effect of aviation sulfate aerosols is readily detected by examining the characteristics of warm clouds. 2050 SC2 emissions produce minimal change in the liquid cloud drop number concentration (Fig. 5e) and liquid water path (Fig. 5g) which are both close to the 2006 aviation emissions level. The perturbations in the ice cloud number

ACPD
doi:10.5194/acp-2015-922

(Fig. 5f) and ice water path (Fig. 5h), on the other hand, are clearly related to the fuel consumption in each emission scenario.

3.3 Regional radiative forcing

Figure 6 illustrates the top of the atmosphere radiative forcing (as the change in the net residual flux at the top of model: RESTOM) in $W\,m^{-2}$ for 2006 (Fig. 6a and c) and 2050 (Fig. 6b and d). Figure 6a and b includes only cirrus (contrail) effects from H_2O and Fig. 6c and d includes cirrus and aerosol effects. 2006 radiative forcing is largest over central Europe and eastern North America. Including aviation aerosols makes the aviation forcing perturbation negative over the oceans (Fig. 6c and d), canceling increases due to contrails. Effects are significantly larger regionally in 2050 as well (Fig. 6b and d). Cooling is more efficient over the ocean due to low albedo from a dark ocean surface.

We focus quantitatively on several key regions, including eastern North America, central Europe, and East Asia. The exact boundaries in these three regions can be found in Table 2. The regions are defined and detailed in Fig. 7, and quantitative estimates of the forcing in each region for the different scenarios are in Table 3.

Contrail cirrus radiative forcing over central Europe in 2050 is projected locally reach 2 $W\,m^{-2}$ (Fig. 7c), which is equivalent to a factor of 2–3 increase from the 2006 level (Table 3). The contrail cirrus radiative forcing over the eastern US (Fig. 7a) could reach 800 $mW\,m^{-2}$ in 2050 and the 2050 increase over 2006 forcing is even higher percentage-wise (Table 3). Nevertheless, the most dramatic increase in contrail cirrus radiative forcing is found in East Asia (an increase of 600 % in 2050BL). This feature is consistent with this region having the largest projected increase in aviation fuel consumption.

When aviation aerosols are also included in the simulations, our simulations indicate that the positive forcing over land is slightly reduced from the forcing induced by contrail cirrus alone (Fig. 7d–f). Similarly as found in Gettelman and Chen (2013) based on the 2006 emissions, the negative forcing induced by aviation emissions is mainly

ACPD
doi:10.5194/acp-2015-922

found over the ocean due to the the low surface albedo. The perturbation is larger over the oceans also because the environment is cleaner (less aerosols) than over land. Over the three regions with the highest air traffic projected in 2050, i.e. eastern US, central Europe, and East Asia, aviation aerosols reduce the regionally-averaged positive radiative forcing induced by contrail cirrus by roughly 50 %, as shown within the blue boxes in Fig. 7. The peak positive forcing within each of the three regions is also reduced by roughly 50 % due to aviation aerosols. Regional estimates are provided in Table 3.

The negative radiative forcing by aviation aerosols found in this study is similar as in Righi et al. (2013). The intensity of the cooling is likely to be dependent on the background cloud drop number concentration.

3.4 Seasonal aviation impacts

Thus far the focus has been annual means, but there is also a seasonal cycle to the aviation radiative forcing. The 2050 contrail cirrus radiative forcing under three aviation emission scenarios exhibits a similar annual cycle (Fig. 8g) as that with the 2006 aviation emission level (Chen and Gettelman, 2013), i.e. higher forcing during the winter months and lower forcing during the summer months in the Northern Hemisphere. The seasonality results from the colder atmospheric temperature in the winter months favoring the formation of contrails (Chen and Gettelman, 2013). The amplitude of the annual cycle of forcing in 2050 is larger than 2006, due to higher aviation emissions in 2050. The three aviation emission scenarios produce similar contrail cirrus radiative forcing, but consistent with Fig. 3a, the baseline scenario has about 10–15 % larger magnitude over the annual cycle. When examining shortwave and longwave radiative forcing separately, however, shortwave radiative forcing reaches its minimum in April (Fig. 8a) and longwave radiative forcing has two maxima in April and November (Fig. 8d).

When aviation aerosols are incorporated in our simulations with aviation water vapor emissions, the magnitude of both the shortwave and longwave radiative forcing become larger (compare Fig. 8b and e with Fig. 8a and d). Note that the short wave is a larger

ACPD
doi:10.5194/acp-2015-922

negative number. The net radiative forcing (Fig. 8h) becomes negative except during the winter months in the Northern Hemisphere in the BL and SC1. In SC2 and SC3 emissions in which there is no sulfate emission, the annual cycle of radiative forcing resembles that of contrail cirrus in Fig. 8g. The stronger induced shortwave forcing in the summer is mainly due to more intense incident solar radiation.

The effect of aviation aerosols is deduced by taking the difference between the two sets of simulations, i.e. the first set which includes only aviation water vapor emissions and the second set which includes both aviation water vapor and aerosol emissions. Since aviation sulfate aerosols are eliminated in SC2 and SC3, the net effect is due to aviation BC alone (half of SC1). It is found that aviation BC produces a slight negative shortwave forcing (Fig. 8c) and positive longwave forcing (Fig. 8f), and its net forcing is nearly zero (Fig. 8i) with a global average of $-4\,\mathrm{mW\,m^{-2}}$ for SC2 and 0 for SC3 (see Tables 3 and 4). Thus, the much stronger forcing found in BL and SC1 is due to the presence of aviation sulfate aerosols. While the longwave forcing exhibits little annual variation (Fig. 8f), the shortwave forcing has a strong annual cycle (Fig. 8c), with the strongest negative forcing during the summer months in the Northern Hemisphere. As illustrated in Fig. 8i, the net forcing of aviation aerosols is mainly controlled by the shortwave.

The signature of contrail cirrus may be readily detected by taking the difference in ice water path (IWP) between the simulation with aviation water vapor emissions and that without (Fig. 9a and b). The increase in IWP is mostly found in regions with high air traffic density, up to $4\,\mathrm{g\,m^{-2}}$. With the background IWP over central Europe and eastern US in the range of $40\,\mathrm{g\,m^{-2}}$ in June–July–August (JJA) and $20\,\mathrm{g\,m^{-2}}$ in December–January–February (DJF), the increase of IWP due to contrail cirrus in 2050 is about 10 % in JJA and 20 % in DJF over these regions. The results also indicate that the enhancement in IWP due to the presence of contrail cirrus is higher during the winter months in the Northern Hemisphere (Fig. 9b) than the summer months (Fig. 9a). This is due to the effect of colder atmospheric temperature in the upper troposphere during the winter which favors the formation of contrails (Chen and Gettelman, 2013). The

ACPD
doi:10.5194/acp-2015-922

inclusion of aviation aerosols is found to further increase IWP (Fig. 9c and d). The deduced effect on IWP by aviation aerosols is illustrated in Fig. 9e and f by taking the difference between simulations with aerosols and contrails, and just contrails. In addition to enhancing IWP where contrail cirrus is present (Fig. 9a and b), the effect of aviation aerosols can spread over high latitudes and into polar regions. This is clearly due to atmospheric transport processes and the lower atmospheric temperature near the cruise altitudes in high latitudes that favors the formation of ice clouds. Note that contrail cirrus forms in flight corridors and a substantial portion of its ice mass originates from the water vapor of the model hydrologic cycle. But aviation aerosols have impacts over their life cycle in the simulations, i.e. they may produce perturbations far from flight corridors since they can be advected long distances.

Sulfate aerosols are highly efficient cloud liquid condensation nuclei, and can enhance liquid cloud drop number and increase liquid water path (LWP) by reducing sedimentation and precipitation as water remains in a larger number of smaller particles. Figure 10 illustrates the mean LWP (Fig. 10a and b) and the effects of aviation water and aerosols. Since contrails have minimal impact on LWP (Fig. 4g), the increase in LWP is mainly due to aviation aerosols. Furthermore, SC2 which eliminates sulfate emissions produces minimal increase in LWP (red line in Fig. 4g), implying most of the increase in LWP is due to aviation sulfate aerosols (compare SC1 and SC2 in Fig. 4g). Note that LWP is found at altitudes well *below* most significant aviation emissions, especially over the oceans. Water only ("contrail cirrus") simulations indicate no significant change in LWP (e.g. Fig. 3g) indicating that aviation water and contrails do not alter LWP. LWP is only enhanced by aviation sulfate aerosol emissions in the simulations (Fig. 10c and d). It is found that largest increase in LWP is typically found where the background LWP and air traffic is large (compare Fig. 10c and d with Fig. 10a and b), which implies that the aviation sulfate aerosols mainly modify the properties of existing clouds instead of creating new clouds. Aviation aerosols emitted at cruise altitude can be transported down to near Earth's surface and thus the aerosol concentration in the lower troposphere can be substantially increased in remote re-

ACPD
doi:10.5194/acp-2015-922

gions. This increase in aerosols in turn raises the cloud drop number concentration of low-level clouds, by about 10 % based on 2050 emission levels. This brightens the existing low-level clouds, known as the Towmey effect (Twomey, 1977). Furthermore, the low-level clouds are found to be more persistent with around 20 % higher in lifetime as indicated by the model variable which records the frequency of the presence of clouds (not shown), due to the presence of aviation sulfate aerosols, known as the Albrecht effect (Albrecht, 1989).

We investigated whether increased aerosol concentration near the Earth's surface are due to aviation emissions transported from the cruise altitude. An experiment was conducted in which all aviation emission below 500 hPa was eliminated in the simulation and the result was nearly identical. This implied that vertical transport of aviation emissions from the cruise altitude down to the lower troposphere was responsible for the observed low-level cloud brightening, but not the aviation emissions during takeoff and landing.

The modification of cloud properties due to the presence of aviation aerosols also generates significant radiative forcing (Fig. 11). The striking similarity in pattern between Figs. 11a and 10c implies that the shortwave radiative forcing due to aviation aerosols is mostly induced by the low-level increases in LWP. The agreement between Figs. 11b and 10d is mainly observed in the tropics because mid and high latitudes do not receive much solar radiation during the winter months in the Northern Hemisphere. The negative shortwave radiative forcing is thus mainly produced by aviation sulfate aerosols since it is in excellent agreement with the increase of LWP.

3.5 Aviation BC

Aviation BC can also modify cloud properties. By comparing the red line (SC2) in Fig. 5g (no Sulfur, 50 % BC) and the green line (BL) in Fig. 4g (no Sulfur or BC), one may conclude that the presence of aviation BC may enhance LWP slightly. Similarly a comparison between Figs. 5h and 4h reveals that aviation BC also enhances IWP in the northern polar regions. Notice the difference in IWP in the Northern polar region

ACPD
doi:10.5194/acp-2015-922

between the green curve in Fig. 4h (2050 BL, H_2O only) and the red curve in Fig. 5h (2050 SC2, BC + H_2O).

To examine the radiative forcing of aviation BC, an experiment with only BC emissions based on 2050 BL was performed and the radiative forcing is illustrated in Fig. 12. The agreement between the two panels indicate that the radiative fluxes at the top of the atmosphere induced by aviation BC is mainly attributed to cloud forcing (indirect effects). The net forcing of aviation BC is positive in high latitudes and polar regions in the Northern Hemisphere, and is negative in the tropics. These effects cancel out and yield nearly zero forcing globally.

4 Summary and conclusions

Four aviation emission scenarios were considered in this study to examine the aviation impact on climate through 2050. The global flight distance is projected to increase by a factor of 4 by 2050 from the 2006 level in all scenarios. The global radiative forcing for contrail cirrus in 2050 level can reach 87 mW m^{-2} which represents a factorial increase of 7 from 2006. Global warming due to anthropogenic greenhouse gases during the 21st century was found to reduce the intensity of contrail cirrus radiative forcing through suppressing the formation of contrails as the upper troposphere gets warmer. Note that the upper tropospheric relative humidity remains nearly constant as the planet warms. Thus stronger warming (in the RCP8.5 scenario) in 2050 results in a larger reduction in contrails than in the RCP4.5 scenario. This result is qualitatively robust across all the aviation scenarios examined.

The aviation emission scenario 1 (SC1), assuming a 2 % gain in engine efficiency per year (i.e. less fuel consumption), was found to have a very minor influence on the contrail cirrus radiative forcing compared to the 2050 BL case. Figure 1 indicates that there is roughly 40 % reduction in fuel consumption in 2050 under SC1 compared with BL, but the reduction of contrail radiative forcing is only about 13 % (see Table 3). This finding indicates that contrail cirrus radiative forcing does not scale linearly with

ACPD
doi:10.5194/acp-2015-922

emission mass which is mainly due to different sensitivities in different regions. Our results also suggest that it is unlikely that the intensity of positive contrail cirrus radiative forcing could be reduced with improvements of engine efficiency.

SC1 with reduced fuel usage, however, significantly reduced the negative forcing induced by aviation sulfate aerosols (Fig. 3b). Nevertheless, even with significant improvements of engine efficiency under SC1, the aerosol cooling still dominates warming by contrail cirrus.

The simulations indicate that SC3, with 5 % increase in aviation water vapor emissions from SC1, produced no significantly different contrail radiative forcing. This is due to the fact that a major portion of ice mass in contrails is from the uptake of water in the ambient atmosphere.

Our simulations indicated that aviation sulfate aerosols produced negative simulated radiative forcing through brightening low-level clouds. Thus, it is worth noting that the induced radiative forcing highly depends on the background cloud distribution which therefore represents an important uncertainty in quantifying the pattern and magnitude of the radiative forcing induced by aviation sulfate aerosols. This also depends on the background aerosol distribution and assumptions made on the physics of aerosol-cloud interactions in contrails.

In summary, CAM simulations indicate that future projected increases in aviation emissions may lead to large increases in contrail radiative forcing and decreases in forcing due to aviation aerosol cooling. There is warming from contrail cirrus, but significant aviation aerosol effects from sulfate result in net cooling, increasing in the future. BC does not have a significant impact on RF. The cooling arises from aerosol effects on LWP well below cruise altitude. These effects have been seen in previous studies with CAM5 (Gettelman and Chen, 2013) and other models (Righi et al., 2013).

However, net positive radiative forcing remains over land, because aerosols are most effective in creating a forcing by brightening clouds over oceans. There are regional effects up to 1–2 $W\,m^{-2}$ over high traffic regions of the Northern Hemisphere. Largest increases in effects between 2006 and 2050 are projected in East Asia where aviation

ACPD
doi:10.5194/acp-2015-922

emissions have the highest regional projected increase. Note that ambient aerosols are decreasing in the future, so effects of aviation aerosols may become more pronounced. Our results indicated minimal sensitivity in contrail cirrus radiative forcing due to fuel consumption (SC1 v. BL). On the other hand, due to the large effects of aviation sulfate aerosol, there is a strong sensitivity to alternative fuels that reduce/eliminate sulfate emissions (SC2). Finally, there is no significant sensitivity to small (5 %) aviation water vapor perturbations.

The climate response to the radiative forcing induced by aviation emissions is beyond the scope of this study. This will be addressed by employing fully coupled simulations by the Community Earth System Model (CESM) and the results will be presented in another paper.

Acknowledgements. This work was funded by the FAA's ATAC Program under award 10-1110-NCAR. Computing resources were provided by the Climate Simulation Laboratory at National Center for Atmospheric Research (NCAR) Computational and Information Systems Laboratory. NCAR is sponsored by the US National Science Foundation. The authors thank Brian Medeiros for his review and Rangasayi Halthore of the FAA for his support.

References

Albrecht, B.: Aerosols, cloud microphysics, and fractionalcloudiness, Science, 245, 1227–1230, 1989. 15

Appleman, H.: The formation of exhaust condensation trails by jet aircraft, B. Am. Meteorol. Soc., 34, 14–20, 1953. 3, 5, 8

Barret, S., Prather, M., Penner, J., Selkirk, H., Balasubramania, S., Dopelheuer, A., Fleming, G., Gupta, M., Halthore, R., Hileman, J., Jacobson, M., Kuhn, S., Lukachko, S., Miake-Lye, R., Petzold, A., Roof, C., Schaefer, M., Schumann, U., Waitz, I., and Wayson, R.: Guidance on the Use of AEDT Griddedaircraft Emissions in Atmospheric Models, version 2.0, Tech. rep., Federal Aviation Administration, 2010. 6, 22

Burkhardt, U. and Kärcher, B.: Global radiative forcing from contrail cirrus, Nature, 1, 54–58, doi:10.1038/NCLIMATE1068, 2011. 3

ACPD

doi:10.5194/acp-2015-922

Chen, C.-C. and Gettelman, A.: Simulated radiative forcing from contrails and contrail cirrus, Atmos. Chem. Phys., 13, 12525–12536, doi:10.5194/acp-13-12525-2013, 2013. 3, 7, 12, 13
Chen, C.-C., Gettelman, A., Craig, C., Minnis, P., and Duda, D. P.: Global contrail coverage simulated by CAM5 with the inventory of 2006 global aircraft emissions, J. Adv. Model. Earth Syst., 4, M04003, doi:10.1029/2011MS000105, 2012. 5, 6, 10
DeMott, P. J., Peters, M. D., Prenni, A. J., Carrico, C. M., Kreidenweis, S. M., Collett Jr., J. L., and Moosmüller, H.: Ice nucleation behavior of biomass combustion particles at cirrus temperatures, J. Geophys. Res., 114, D16205, doi:10.1029/2009JD012036, 2009. 3
Demott, P. J., Prenni, A. J., Liu, X., Kreidenweis, S. M., Petters, M. D., Twohy, C. H., Richardson, M. S., Eidhammer, T., and Rogers, D. C.: Predicting global atmospheric ice nuclei distribution and their impacts on climate, P. Natl. Acad. Sci. USA, 107, 11217–11222, 2010. 3
Dietmüller, S., Ponater, M., Sausen, R., Hoinka, K.-P., and Pechtl, S.: Contrails, natural clouds, and diurnal temperature range, J. Climate, 21, 5061–5075, doi:10.1175/2008JCLI2255.1, 2011. 3
Gettelman, A. and Chen, C.-C.: The climate impact of aviation aerosols, Geophys. Res. Lett., 40, L50520, doi:10.1002/grl.50520, 2013. 3, 5, 7, 9, 11, 17
Gettelman, A., Fetzer, E. J., Irion, F. W., and Eldering, A.: The global distribution of supersaturation in the upper troposphere, J. Climate, 19, 6089–6103, 2006. 5
Gettelman, A., Liu, X., Ghan, S. J., Morrison, H., Park, S., Conley, A. J., Klein, S. A., Boyle, J., Mitchell, D. L., and Li, J.-L.: Global simulations of ice nucleation and ice supersaturation with an improved cloud scheme in the Community Atmosphere Model, J. Geophys. Res., 115, D18216, doi:10.1029/2009JD013797, 2010. 4
Hendricks, J., Kärcher, B., Lohmann, U., and Ponater, M.: Do aircraft black carbon emissions affect cirrus clouds on the global scale?, Geophys. Res. Lett., 32, L12814, doi:10.1029/2005GL022740, 2005. 3
Hendricks, J., Kärcher, B., and Lohmann, U.: Effects of ice nuclei on cirrus clouds in a global climate model, J. Geophys. Res., 116, D18206, doi:10.1029/2010JD015302, 2011. 3
IPCC: Aviation and Global Atmosphere, edited by: Penner, J. E., Lister, D. H., Griggs, D. J., Dokken, D. J., and MacFarland, M., Cambridge University Press, Cambridge UK, 373 pp., 1999. 2
IPCC: Climate Change 2013: The Physical Science Basis. Working Group 1 (WG)1 Contribution to the Intergovernmental Panel on Climate Change (IPCC) 5th Assessment Report (AR5), edited by: Stocker, T. F., Qin, D., Plattner, G.-K., Tignor, M. M. B., Allen, S. K.,

ACPD
doi:10.5194/acp-2015-922

Boschung, J., Nauels, A., Xia, Y., Bex, V., and Midgley, P. M., Cambridge University Press, Cambridge, UK, 2013.

Lee, D. S., Fahey, D. W., Forster, P. M., Newton, P. J., Wit, R. C. N., Lim, L. L., Owen, B., and Sausen, R.: Aviation and global climate change in the 21th century, Atmos. Environ., 43, 3520–3537, doi:10.1016/j.atmosenv.2009.04.024, 2009. 2, 4

Liu, X., Penner, J. E., and Wang, M.: Influence of anthropogenic sulfate and black carbon on upper tropospheric clouds in the NCAR CAM3 model coupled to the IMPACT global aerosol model, J. Geophys. Res., 114, D03204, doi:10.1029/2008JD010492, 2009. 4

Liu, X., Easter, R. C., Ghan, S. J., Zaveri, R., Rasch, P., Shi, X., Lamarque, J.-F., Gettelman, A., Morrison, H., Vitt, F., Conley, A., Park, S., Neale, R., Hannay, C., Ekman, A. M. L., Hess, P., Mahowald, N., Collins, W., Iacono, M. J., Bretherton, C. S., Flanner, M. G., and Mitchell, D.: Toward a minimal representation of aerosols in climate models: description and evaluation in the Community Atmosphere Model CAM5, Geosci. Model Dev., 5, 709–739, doi:10.5194/gmd-5-709-2012, 2012. 4

Minnis, P., Young, D. F., Garber, D. P., Nguyen, L., Smith, W. L. J., and Palikonda, R.: Transformation of contrails into cirrus during SUCCESS, Geophys. Res. Lett., 25, 1157–1160, 1998. 3

Morrison, H. and Gettelman, A.: A new two-moment bulk stratiform cloud microphysics scheme in the Community Atmospheric Model (CAM3), Part I: description and numerical tests, J. Climate, 21, 3642–3659, 2008. 4

Neale, R. B., Chen, C.-C., Gettelman, A., Lauritzen, P. H., Park, S., Williamson, D. L., Conley, A. J., Garcia, R., Kinnison, D., Lamarque, J.-F., Marsh, D., Mills, M., Smith, A. K., Tilmes, S., Vitt, F., Morrison, H., Cameron-Smith, P., Collins, W. D., Iacono, M. J., Easter, R. C., Ghan, S. J., Liu, X., Rasch, P. J., and Taylor, M. A.: Description of the NCAR Community Atmosphere Model (CAM 5.0), NCAR Technical Note, NCAR/TN-486+STR, available at: http://www.cesm.ucar.edu/models/cesm1.0/cam/docs/description/cam5_desc.pdf (last access: November 2012), 2010. 4

Penner, J. E., Chen, Y., Wang, M., and Liu, X.: Possible influence of anthropogenic aerosols on cirrus clouds and anthropogenic forcing, Atmos. Chem. Phys., 9, 879–896, doi:10.5194/acp-9-879-2009, 2009. 3

Ponater, M., Marquart, S., and Sausen, R.: Contrails in a comprehensive global climate model: parameterization and radiative forcing results, J. Geophys. Res., 107, ACL2.1–ACL2.15, doi:10.1029/2001JD000429, 2002. 5

ACPD

doi:10.5194/acp-2015-922

Rap, A., Forster, P. M., Jones, A., Boucher, O., Haywood, J. M., Bellouin, N., and De Leon, R. R.: Parameterization of contrails in the UK Met Office Climate Model, J. Geophys. Res., 115, D10205, doi:10.1029/2009JD012443, 2010. 3

Rasch, P. J., Latham, J., and Chen, C.-C.: Geoengineering by cloud seeding: influence on sea-ice and climate system, Environ. Res. Lett., 4, 045112, doi:10.1088/1748-9326/4/4/045112, 2009.

Righi, M., Hendricks, J., and Sausen, R.: The global impact of the transport sectors on atmospheric aerosol: simulations for year 2000 emissions, Atmos. Chem. Phys., 13, 9939–9970, doi:10.5194/acp-13-9939-2013, 2013. 3, 12, 17

Twomey, S.: The influence of pollution on the shortwave albedo of clouds, J. Atmos. Sci., 34, 1149–1152, 1977. 15

Schmidt, E.: Die Entstehung von Eisnebel aus den Auspuffgasen von Flugmotoren, Schriften der Deutschen Akademie der Luftfahrtforschung, 44, 1–15, 1941. 3, 5, 8

Schröder, F., Kärcher, B., Duroure, C., Strom, J., Petzold, A., Gayet, J.-F., and Strauss, B.: On the transition of contrails into cirrus clouds, J. Atmos. Sci., 57, 464–480, 2000. 6

Schumann, U.: On conditions for contrail formation from aircraft exhausts, Meteorol. Z., 5, 4–24, 1996. 5

Schumann, U. and Graf, K.: Aviation-induced cirrus and radiation changes at diurnal timescales, J. Geophys. Res., 118, 2404–2421, doi:10.1002/jgrd.50184, 2013. 3

Schumann, U. and Wendling, P.: Determination of contrails from satellite data and observational results, in: Proc. of a DLR Intern. Coll., 15 and 16 November 1990, Lecture Notes in Engineering, 60, Spinger-Verlag, Berlin, 138–153, 1990. 3

Van Vuuren, D. P., Edmonds, J., Kainuma, M., Riahi, K., Thomson, A., Hibbard, K., Hurtt, G. C., Kram, T., Krey, V., Lamarque, J.-F., Masui, T., Meinshauusen, M., Nakicenovic, N., Smith, S. J., and Rose, S. K.: The representative concentration pathways: an overview, Climatic Change, 109, 5–31, 2011. 7

ACPD

doi:10.5194/acp-2015-922

Table 1. Various aviation emission scenarios based on Barrett et al. (2010).

Year	Name	Description
2006	AIR	aviation emissions based on observed data in 2006
2016, 2026, 2036, 2050	BL	Baseline projected aviation emissions in 2016, 2026, 2036, 2050
2016, 2026, 2036, 2050	SC1	Scenario 1, lower fuel use assuming 2 % efficiency improvement per year
2016, 2026, 2036, 2050	SC2	Scenario 2, SC1 with no sulfate and 50 % BC emissions
2016, 2026, 2036, 2050	SC3	Scenario 3, SC2 with 5 % increase in emitted water

ACPD
doi:10.5194/acp-2015-922

Table 2. Vertices of eastern North America, central Europe, and East Asia denoted by blue boxes in Fig. 7.

Eastern North America	Central Europe	East Asia
(95° W, 45° N)	(5° W, 58° N)	(100° E, 43° N)
(58° W, 45° N)	(23° E, 58° N)	(150° E, 43° N)
(95° W, 26° N)	(5° W, 45° N)	(92° E, 11° S)
(68° W, 26° N)	(23° E, 58° N)	(115° E, 11° S)

ACPD
doi:10.5194/acp-2015-922

Table 3. Radiative forcing (mW m^{-2}) due to aviation H_2O emissions.

meteorology	emission scenario	global	N. America	C. Europe	E. Asia
present	2006AIR	12	195	483	41
2050RCP4.5	2050BL	87	798	1682	272
2050RCP4.5	2050SC1	76	724	1568	231
2050RCP4.5	2050SC2	76	724	1568	231
2050RCP4.5	2050SC3	80	681	1952	213
2050RCP8.5	2050BL	83	852	1558	248
2050RCP8.5	2050SC1	73	777	1442	211
2050RCP8.5	2050SC2	73	777	1442	211
2050RCP8.5	2050SC3	75	865	1597	221

ACPD
doi:10.5194/acp-2015-922

Table 4. Radiative forcing (mW m^{-2}) due to aviation H_2O + BC + SO_4 emissions. Note that there is no aviation sulfate aerosols in SC2 and SC3.

meteorology	emission scenario	global	N. America	C. Europe	E. Asia
present	2006AIR	−22	117	407	15
2050RCP4.5	2050BL	−71	491	1301	13
2050RCP4.5	2050SC1	−28	514	1284	57
2050RCP4.5	2050SC2	73	754	1483	173
2050RCP4.5	2050SC3	76	728	1824	160
2050RCP8.5	2050BL	−77	363	868	44
2050RCP8.5	2050SC1	−32	417	920	80
2050RCP8.5	2050SC2	69	804	1320	151
2050RCP8.5	2050SC3	75	871	1601	149

ACPD
doi:10.5194/acp-2015-922

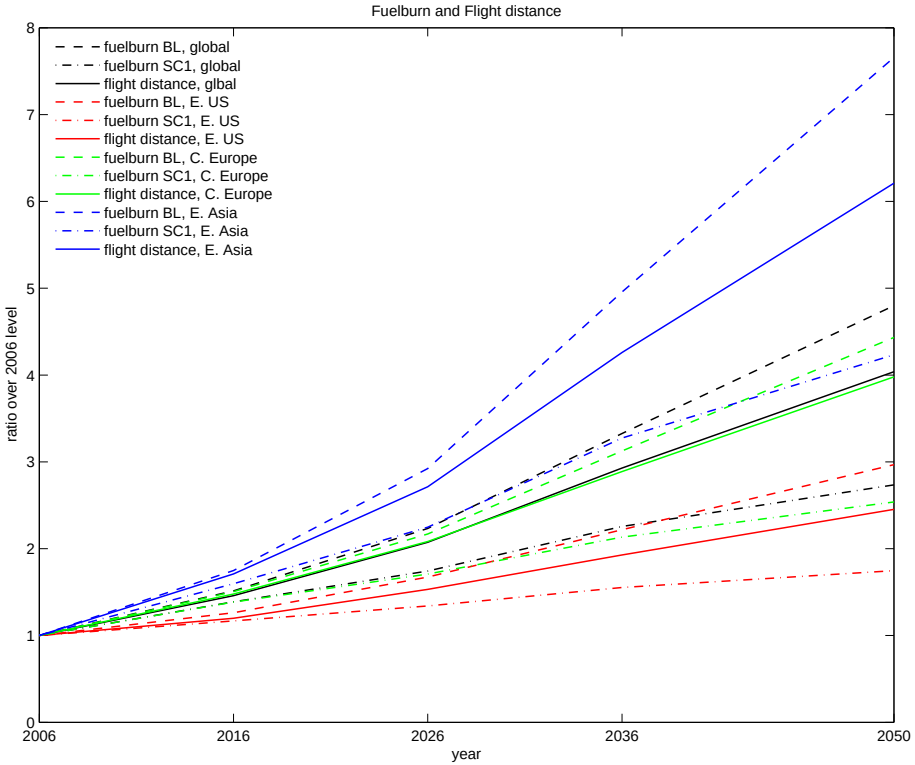

Figure 1. Global and regional flight distance and fluelburn under two future scenarios, Baseline and Scenario 1, over the 2006 level. The regions over eastern US, central Europe and East Asia are depicted by the blue boxes in Fig. 7.

ACPD
doi:10.5194/acp-2015-922

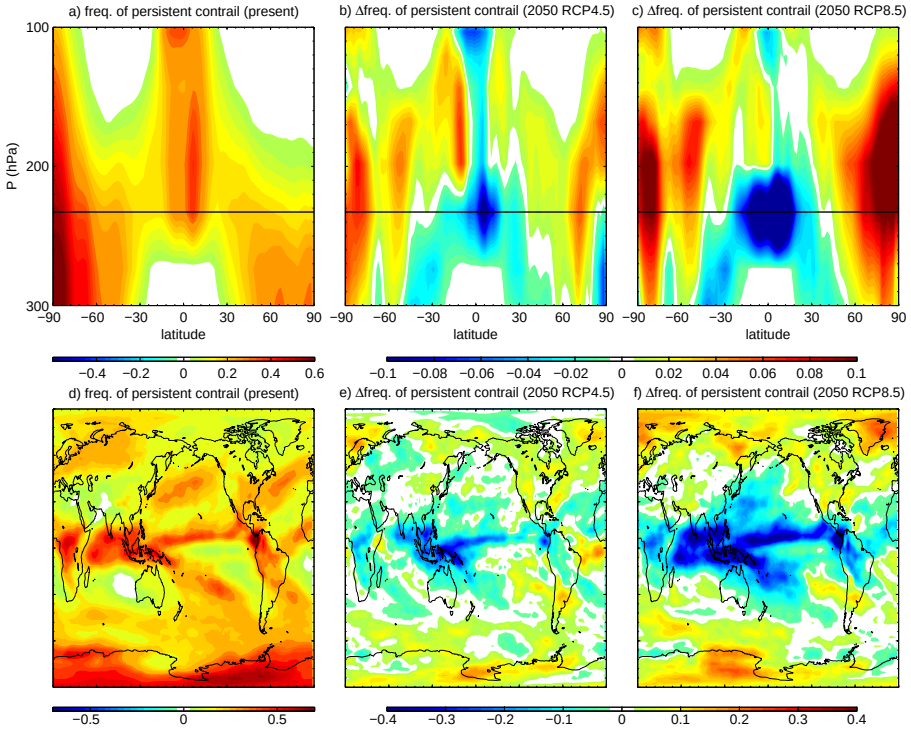

Figure 2. Frequency of persistent contrail based on present and future (RCP4.5 in 2050 and RCP8.5 in 2050) meteorologies: **(a)** zonal average between 100 and 300 hPa, **(b)** zonal difference between 2050 of RCP4.5 and present, **(c)** zonal difference between 2050 of RCP8.5 and present, **(d)** the present condition at P = 232 hPa, **(e)** difference between 2050 of RCP4.5 and present at P = 232 hPa, and **(f)** difference between 2050 of RCP8.5 and present.

ACPD
doi:10.5194/acp-2015-922

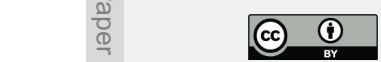

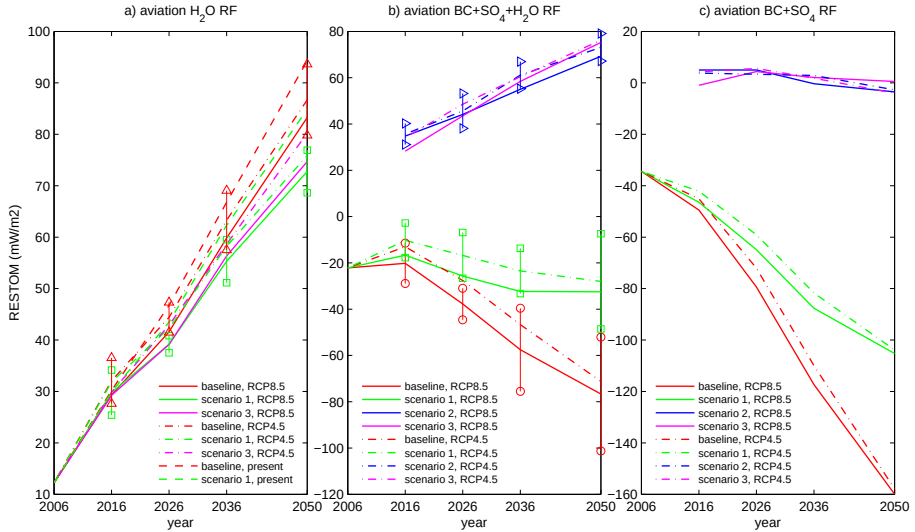

Figure 3. Time series of globally averaged radiative forcing in mW m^{-2} based on various aviation emissions scenarios and background meteorologies due to: **(a)** contrail cirrus only, **(b)** contrail cirrus and aviation aerosols, and **(c)** aviation aerosols, deduced by the difference between **(a)** and **(b)**. RESTOM denotes the change in the net residual radiative flux at the top of model. Note that in **(b)** and **(c)**, there is no aviation sulfate aerosols in scenarios 2 and 3.

ACPD
doi:10.5194/acp-2015-922

Future aviation radiative forcing

C.-C. Chen and A. Gettelman

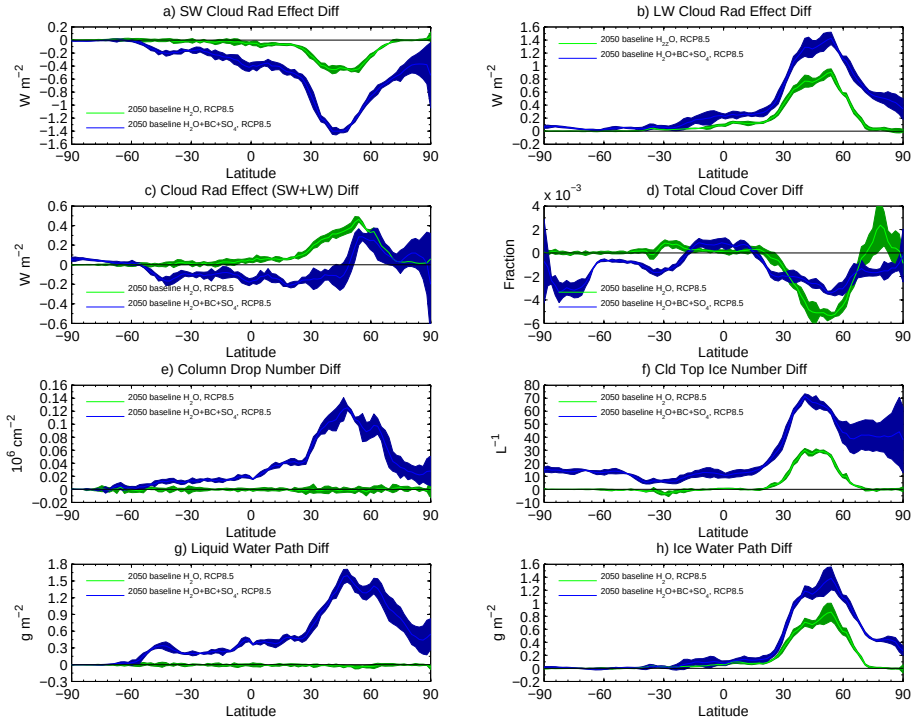

Figure 4. Zonally averaged aviation impact with the green line representing water vapor emissions only of Baseline in 2050 and the blue line representing water vapor and aviation aerosols of Baseline in 2050, both coupled with the background meteorology in 2050 by RCP8.5: **(a)** shortwave cloud forcing, **(b)** longwave cloud forcing, **(c)** net cloud forcing, **(d)** total cloud difference, **(e)** column drop number difference, **(f)** cloud top ice number difference, **(g)** liquid water path difference, and **(h)** ice water difference. The spread of each curve represent the two standard deviations from the four-member ensemble of each case.

ACPD
doi:10.5194/acp-2015-922

Future aviation radiative forcing

C.-C. Chen and A. Gettelman

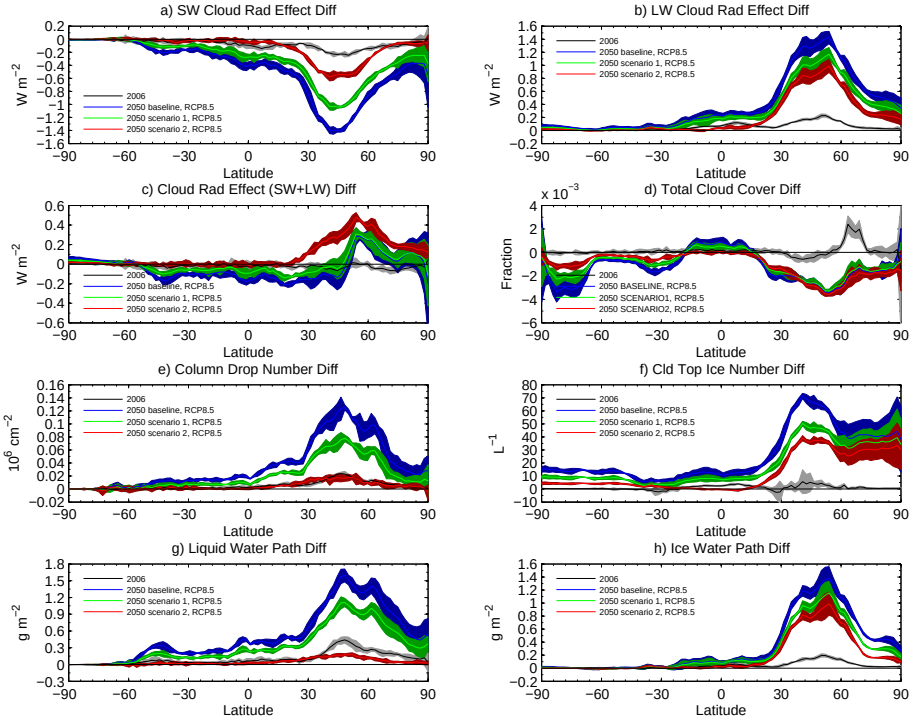

Figure 5. Similar as in Fig. 4, zonally averaged aviation impact due to contrail cirrus and aviation aerosols based on emissions in 2006 and the present background meteorology, three future emissions scenarios in 2050 (Baseline, Scenarios 1 and 2) and the background meteorology in 2050 by RCP8.5.

ACPD
doi:10.5194/acp-2015-922

Future aviation radiative forcing

C.-C. Chen and A. Gettelman

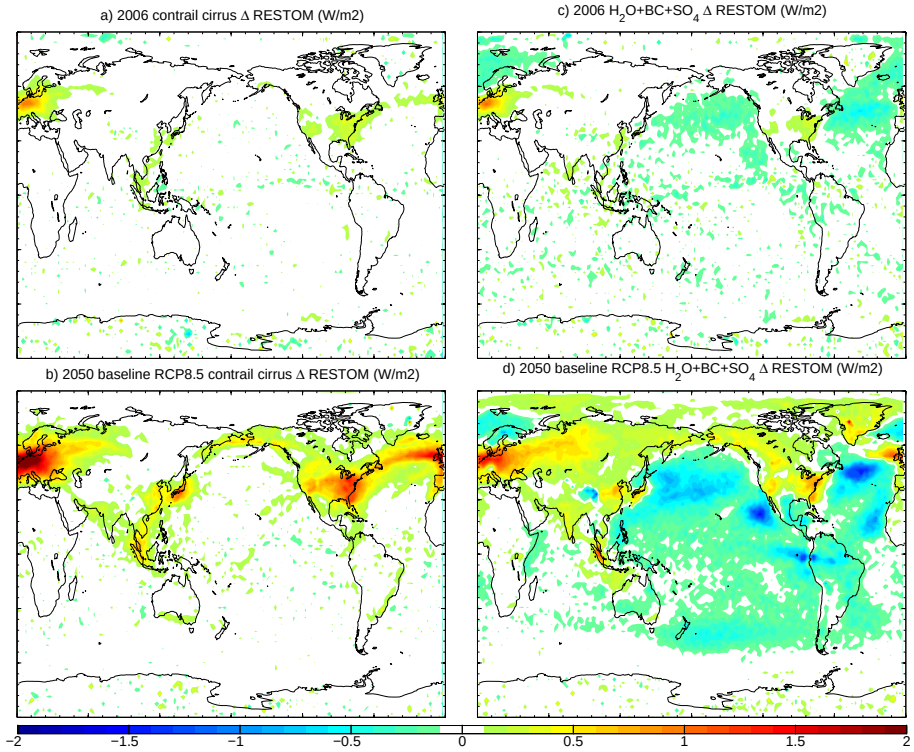

Figure 6. Regional radiative forcing in W m^{-2} due to: **(a)** contrail cirrus in 2006 with present day meteorology, **(b)** contrail cirrus and aviation aerosols in 2006 with present day meteorology, **(c)** contrail cirrus in 2050 with RCP8.5 2050 meteorology, and **(d)** contrail cirrus and aviation aerosols in 2050 with RCP8.5 2050 meteorology. Aviation emissions are based on the Baseline emission scenario.

ACPD
doi:10.5194/acp-2015-922

Future aviation radiative forcing

C.-C. Chen and A. Gettelman

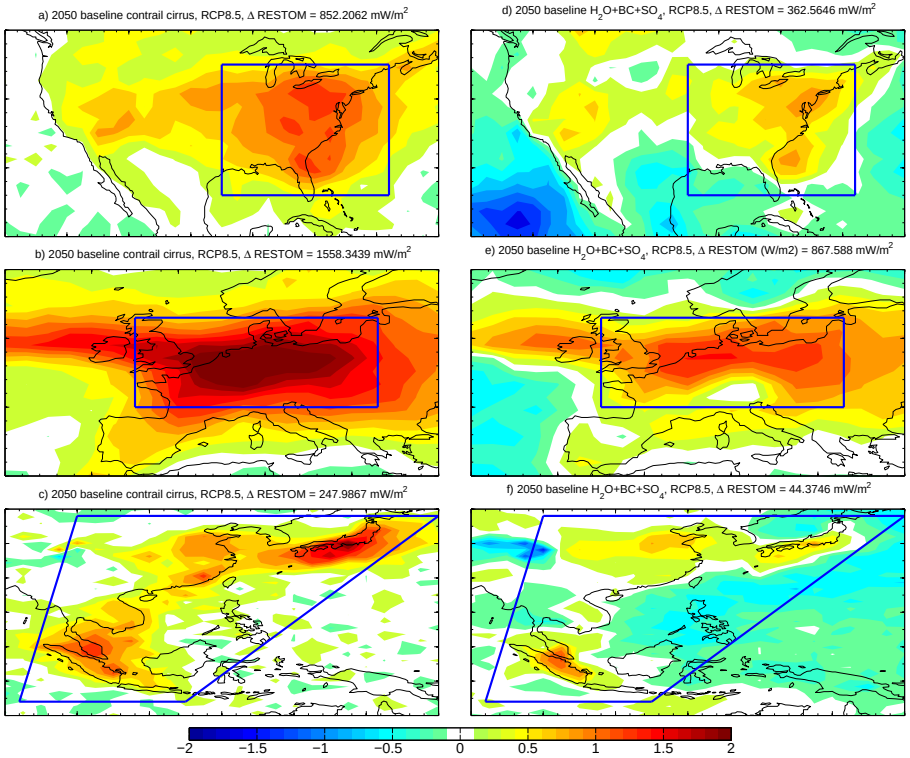

Figure 7. Regional radiative forcing in W m^{-2} based on the Baseline emission scenario in 2050 with RCP8.5 2050 meteorology due to contrail cirrus **(a–c)** and contrail cirrus and aviation aerosols **(d–f)**. The box averages are given in the title of each panel.

ACPD
doi:10.5194/acp-2015-922

Future aviation radiative forcing

C.-C. Chen and A. Gettelman

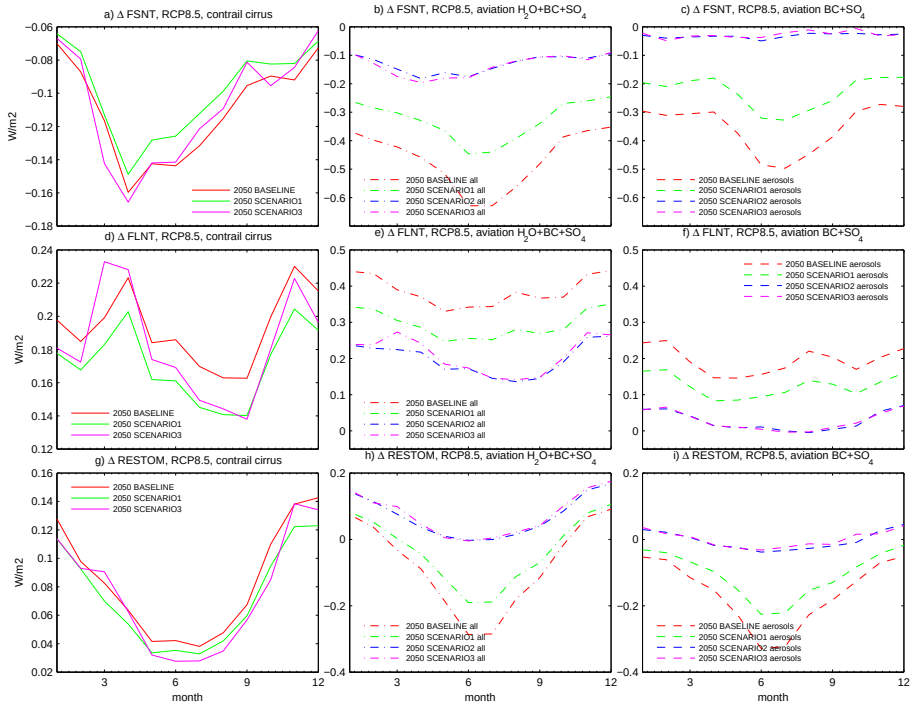

Figure 8. Annual cycle of globally averaged shortwave (FSNT: **a–c**), longwave (FLNT: **d–f**) and net (RESTOM: **g–i**) radiative forcing in $W\,m^{-2}$ at the top of the atmosphere due to contrail cirrus **(a, d, g)**, contrail cirrus and aviation aerosols **(b, e, h)**, and aviation aerosols **(c, f, i)** based on three aviation emission scenarios in 2050 with RCP8.5 2050 meteorology.

ACPD
doi:10.5194/acp-2015-922

Future aviation radiative forcing

C.-C. Chen and A. Gettelman

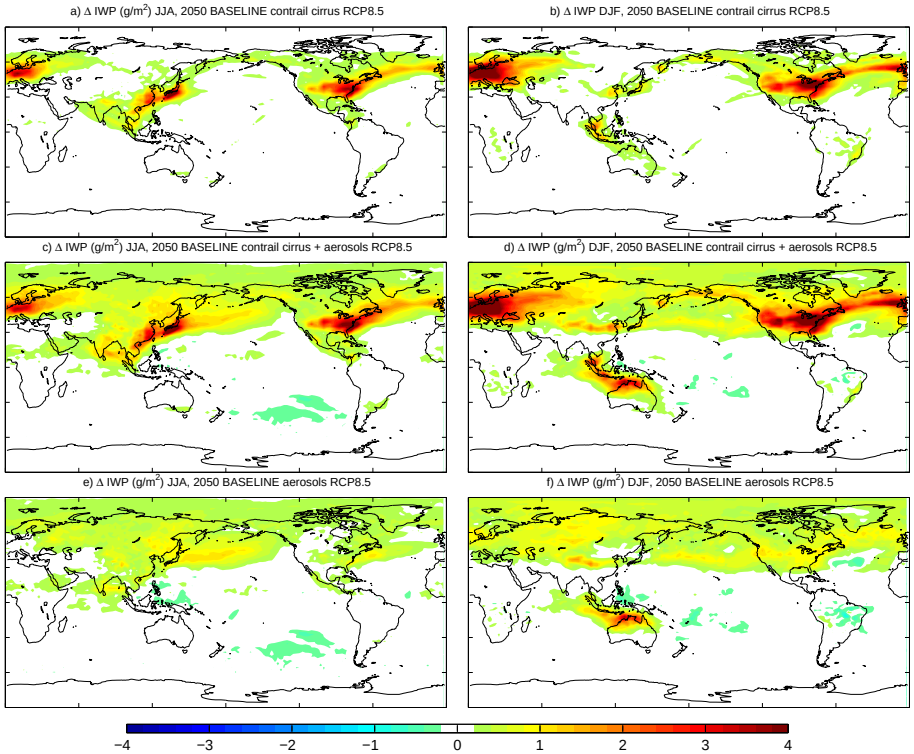

Figure 9. Seasonally averaged (JJA: **a, c, e**, DJF: **b, d, f**) ice water path difference in g m^{-2} due to contrail cirrus **(a, b)**, contrail cirrus and aviation aerosols **(c, d)**, and aviation aerosols **(e, f)** based on the 2050 Baseline emissions with RCP8.5 2050 meteorology.

ACPD
doi:10.5194/acp-2015-922

Future aviation radiative forcing

C.-C. Chen and A. Gettelman

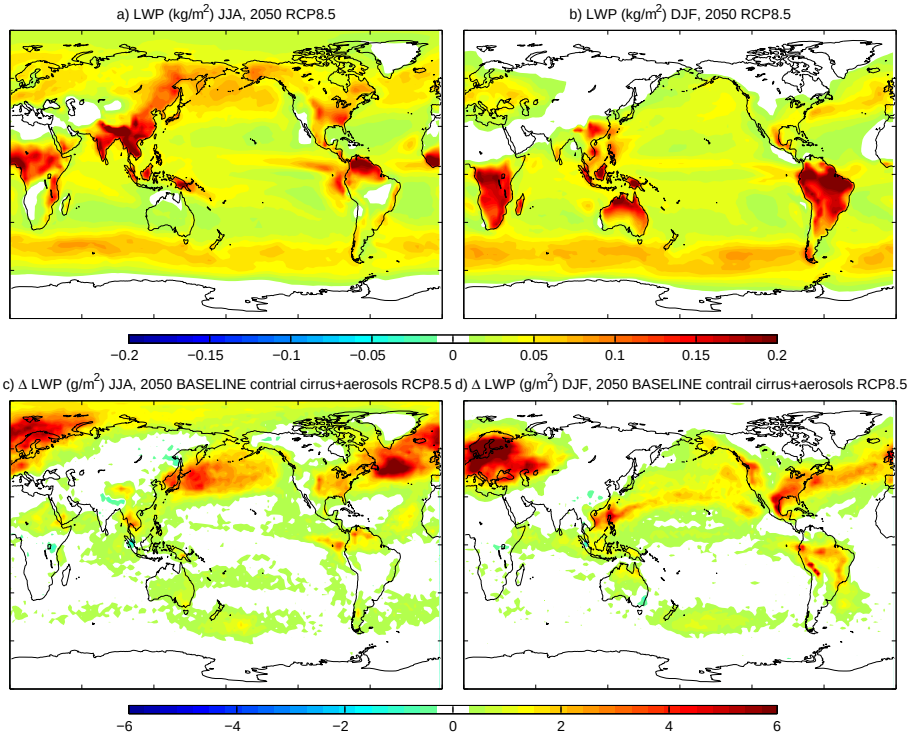

Figure 10. Seasonally averaged liquid water path in g m^{-2}: **(a)** JJA background field of RCP8.5 2050 meteorology, **(b)** DJF background field of RCP8.5 2050 meteorology, **(c)** JJA difference due to contrail cirrus and aviation aerosols in 2050, **(d)** DJF difference due to contrail cirrus and aviation aerosols in 2050.

ACPD
doi:10.5194/acp-2015-922

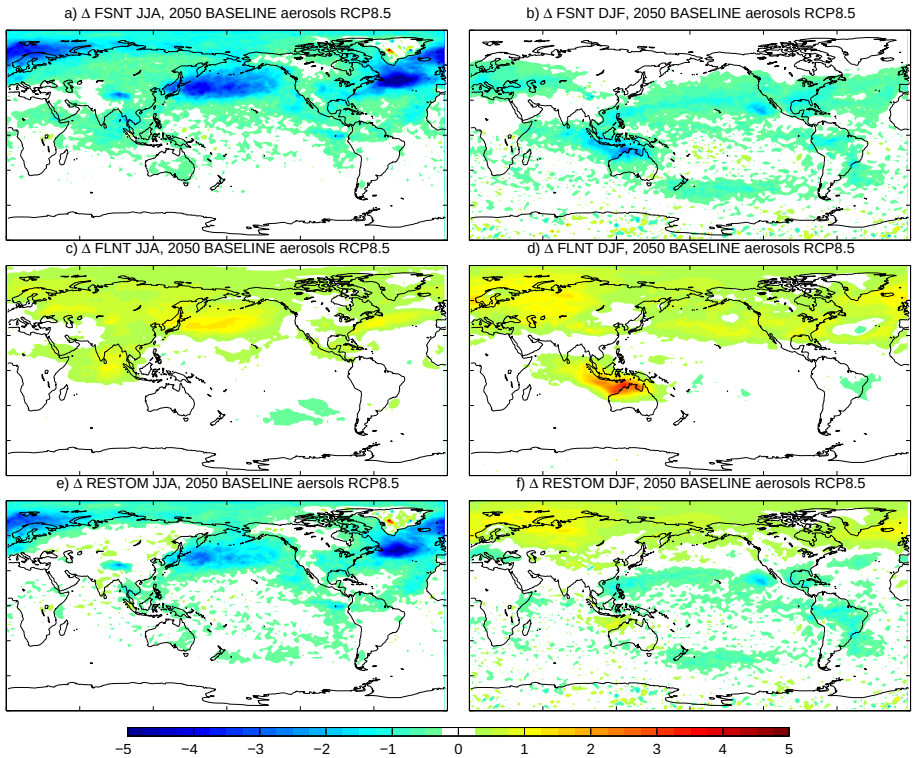

Figure 11. Seasonally averaged shortwave (FSNT: **a, b**), longwave (FLNT: **c, d**), and net (RESTOM: **e, f**) radiative forcing in mW m^2 at the top of the atmosphere due to 2050 Baseline aviation aerosols with RCP8.5 2050 meteorology.

ACPD
doi:10.5194/acp-2015-922

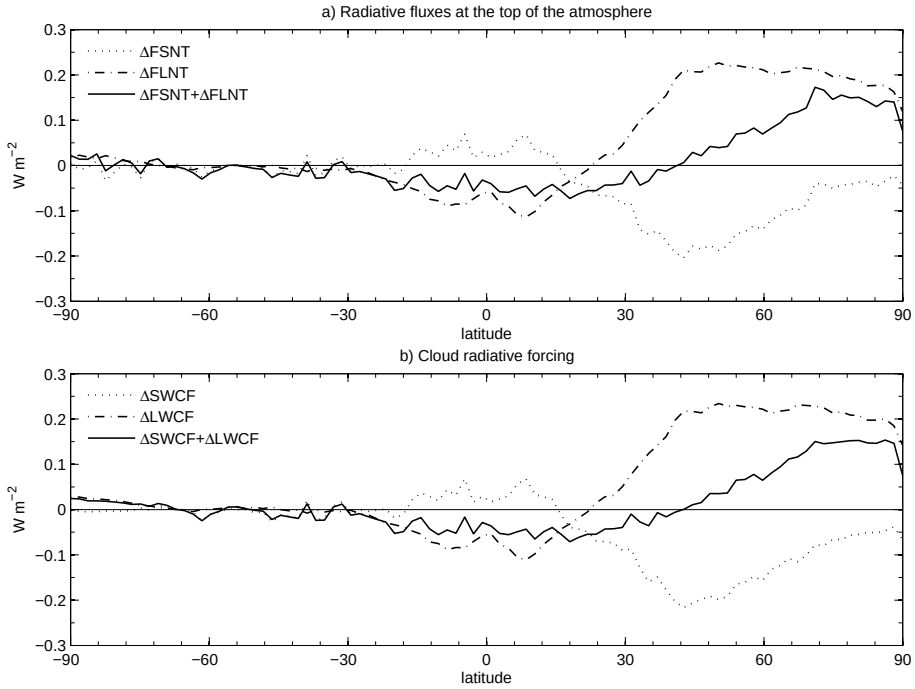

Figure 12. Zonal average of radiative fluxes at the top of the atmosphere energy balance (shortwave: FSNT, longwave: FLNT) and cloud radiative forcing (shortwave: SWCF, longwave: LWCF) in mW m^{-2} due to aviation BC based on 2050BL emissions with 2050 RCP8.5 meteorology.

ACPD
doi:10.5194/acp-2015-922